MRI Acquisition and Analysis Protocol for *In Vivo* Intraorbital Optic Nerve segmentation at 3T

"Technical Developments"

Advance(s) in Knowledge (up to five points):

1) This pilot study proposes a new MRI acquisition and analysis protocol that allows for the first time reliable and reproducible segmentation of the entire intraorbital optic nerve mean cross-sectional area *in vivo* using a 3T MR system.
2) The MRI acquisition protocol presented here can be readily implemented in the clinical setting without additional MR system hardware/software modifications and can be acquired within clinically acceptable scan times.
3) The MRI acquisition and analysis protocol presented here in healthy controls can be used to study diseases of the optic nerve that are known to be associated with axonal loss and progressive atrophy.

In summary, this study defines a new MRI acquisition and analysis protocol that allows for the first time reliable and reproducible measurement of the mean cross-sectional area of the entire intraorbital optic nerve *in vivo* at 3T.

ABSTRACT

Purpose: To present a new acquisition and analysis protocol for reliable and reproducible segmentation of the entire intraorbital optic nerve (ION) mean cross-sectional area by means of magnetic resonance imaging (MRI) at 3 tesla (T).

Materials and Methods: 8 healthy volunteers (mean age 31, 5 male) gave written informed consent and both their IONs were imaged individually using a coronal-oblique T2-weighted fast multi-dynamic image acquisition scheme; the proposed acquisition scheme has its rationale in registering and averaging repeated acquisitions of the same field of view, to account for motion related artefacts commonly associated with longer acquisitions. Mean cross-sectional area of each ION was measured using a semi-automated image analysis protocol that was based on an active surface model previously described and used for spinal cord imaging. Reproducibility was assessed for repeated scans (scan-rescan) and repeated image analysis performance (intra-observer).

Results: Mean and standard deviation values of the left ION cross-sectional area for the 8 healthy volunteers was 5.0 (± 0.7) mm^2 and for the right ION was 5.3 (± 0.8) mm^2. Mean scan-rescan COV for the left ION was 4.3% and for the right was 4.4%. Mean intra-observer COV for the left ION was 2.1% and for the right was 1.8%.

Conclusion: This study presents a new MRI acquisition and analysis protocol for reliable and reproducible *in vivo* measurement of the entire ION mean cross-sectional area as

demonstrated in a pilot study of healthy subjects. The protocol presented here can be used in future studies of the ION in disease state.

INTRODUCTION

In vivo magnetic resonance imaging (MRI) protocols that allow reliable segmentation and measurement of the mean cross-sectional area of the entire intraorbital optic nerve (ION) can be very important when studying neurological conditions such as glaucoma (1-4) and multiple sclerosis (MS) (5-8). This is because these pathological conditions are known to involve axonal loss and progressive atrophy, with a consequent reduction in the mean cross-sectional area of the ION. Reliable measurement of such changes not only would aid in the early diagnosis of disease severity, but could also be invaluable when assessing neuroprotective strategies.

The ION mean cross-sectional area has been measured over a portion of it by means of semi-automated image analysis of high-resolution MR images acquired with a variety of pulse sequences and image contrast, yet with varying results (5, 9-14). While the image analysis methods currently employed for segmenting the ION predominantly suffer from operator dependent errors, image acquisition strategies can be considered the more problematic aspect influencing reproducibility. For example, the higher the spatial resolution required is, the longer it takes to acquire the images with consequent motion artefacts affecting especially the anterior portion of the ION (5); faster acquisition strategies, instead, may depict the anterior portion of the ION more clearly but can suffer from lack of conspicuity in the distal portion (12). Single-slice ultra-fast acquisition methods at different orthogonal positions along the length of the ION have also been employed successfully, accurately addressing motion related effects (10, 11). However,

single-slice acquisitions may not be suitable in situations where the assessment of a representative length of the ION is desired; given the variation in length of the ION between subjects (15), coupled with the possibility of disease manifestation (e.g. atrophy due to axonal loss) at inconsistent sections along the length of ION, it would be more desirable to acquire contiguous slices throughout the entire ION in a single imaging session.

In this work we propose both a new image acquisition and segmentation method to cover the entire length of the ION which takes into account the technical challenges associated with imaging the ION and is based on a) a fast multi-dynamic image acquisition scheme that combines separately acquired volumes and registering them to each other to account for motion related artefacts and b) a semi-automated image analysis method that is less operator dependent than other proposed methods, and which is based on an active surface model (ASM) that has been shown to be invaluable for measuring the spinal cord cross-sectional area (16), a small and discrete structure similar to the ION.

MATERIALS AND METHOD

Study participants

Eight healthy volunteers were recruited (mean age 31 years, range 29-33, 5 male). Written informed consent was obtained from all participants. This work was approved by our local research ethics committee.

MR imaging

A 3 tesla (T) Philips Achieva MRI system (Philips Healthcare, Best, Netherlands) was used for this study with the manufacturer's product 32-channel head coil. For each healthy subject, the left and right ION were imaged individually in the coronal-oblique plane to ensure the slices were orthogonal to the ION longitudinal axis in all cases; for consistent prescription of the main acquisition volume, the second slice of the volume was always positioned adjacent to the globe and this was facilitated by high resolution reference images acquired in the sagittal and axial planes through the level of both optic nerves (see Figure 1). The following MR sequence parameters were used for the main acquisition: A fat-suppressed heavily T2-weighted multi-slice 'single-shot' 2D-TSE with TR = 16 seconds; TE = 74 ms; flip angle $\alpha = 90°$; FOV= 160 x 160 mm^2; voxel size = 0.5 x 0.5 x 3 mm^3; NEX = 1; 20 contiguous slices (no gap); scanning time = 32 seconds per dynamic scan; number of repeated dynamic scans = 15 (total scan time 8 minutes per ION); the individual volumes acquired were then registered and added to produce the final image that was used for image segmentation and cross-sectional area measurements of the ION (see next section on 'Image analysis protocol' for further details).

In order to minimise the effect of physical motion of the optic nerve during acquisition, the volunteers were verbally instructed by the MR operator to focus their vision on a coloured marker positioned in front of them (i.e. straight gaze) for each one of the 32 second dynamic scans, with a short break in-between each dynamic scan.

Image analysis protocol

Image registrations

The 15 separately acquired volumes were registered slice-by-slice using the intensity-based 2D image registration options provided by the 'imregister' command in MATLAB 2012a (Mathworks, Natick, MA, USA). Prior to the registrations, all the images were cropped to a matrix size of 31 x 31 pixels (see Figure 2); this was deemed necessary due to the uncoupled motion of the ON compared to surrounding structures. A further consequence of the cropping was a considerable reduction in processing time. Using the first volume as reference, corresponding slices from each volume were then registered slice-by-slice using a 2D rigid transformation with bilinear interpolation (i.e. the transformation consisted of translation and rotation) and averaged to produce a single volume for each ION. As an example of the degree of misalignment encountered between slices prior to registration, Figure 3 a) demonstrates the same slice taken from each volume (in this example slice 2, i.e. proximal 3 mm to the globe), binarized using the Otsu's method (17), interpolated to a higher resolution for better display and added to produce a single image; Figure 3 b) shows the final processed image.

Cross-sectional area measurements

Using the Jim Software (Xinapse systems, www.xinapse.com), the ASM segmentation option was employed to segment 8-10 slices starting immediately behind the globe up to the orbital apex; the apex level was determined by visual inspection using high resolution sagittal images as a reference and the number of slices depended on the length of the ION between the globe and the orbital apex in each subject. Figure 4 shows an example of how the boundary of the ION was identified using the ASM segmentation option. Initially, seed points were positioned within the ION on consecutive slices and the ION contours were then identified using the ASM algorithm; following segmentation, contours were visually inspected and manually edited whenever necessary.

Reproducibility study

Scan-rescan reproducibility was assessed by repeating the MR imaging protocol 3 times on 5 out of 8 volunteers, on separate occasions (with a minimum of 7 days and a maximum of 14 days interval between measurements), and with one experienced rater analysing all the data. In order to assess the intra-observer reproducibility, the same rater re-analysed all the data from the 5 volunteers' first visit 3 times (with the analysis performed on separate occasions after a period of at least 2 weeks in between each analysis).

Statistical analysis

Statistical analysis was performed using the SPSS 11.0 statistical package (SPSS, Chicago, Ill., USA). For the assessment of scan-rescan and intra-observer reproducibility, the coefficient of variation (COV), expressed as a percentage, was calculated using the

mean and standard deviations from the repeated measures using the equation %COV=100 x [SD/mean]. For those study participants whose ION had the same length, scan-rescan COV values were reported both as an average across all slices but also on a slice by slice. Differences between left and right ION mean cross-sectional areas were investigated using paired t-tests and significance was accepted at $p < 0.05$.

RESULTS

Image analysis was performed using all datasets without any exclusion due to motion or other artefacts. On average, image processing, which included segmentation and cross-sectional area measurements of each ION, required less than 10 minutes per side to perform for a total of 20 minutes per subject. Less than 20% of the contours identified using ASM required manual editing.

Mean and standard deviation (SD) of the left ION cross-sectional area for the 8 healthy volunteers was 5.0 (± 0.7) mm^2 and for the right ION was 5.3 (± 0.8) mm^2. Mean scan-rescan COV for the left ION was 4.3% and for the right 4.4%. Mean intra-observer COV for the left ION was 2.1% and for the right 1.8%. Table 1 shows more detailed results pertaining to individual sections of the left and right ION. In fact, results from the scan-rescan reproducibility assessment are shown for each individual section of the ION (i.e. slice by slice) for a better account on the effectiveness of the method in detecting possible localized changes. In addition, the table shows that the mean cross-sectional area of the ION reduces as it extends from immediately behind the globe towards the orbital apex.

Statistical comparisons of mean cross-sectional area values between the left and right ION were not found to be significant.

DISCUSSION

The ability to measure the ION cross-sectional area can be invaluable when assessing certain pathological conditions (1-8). However, current methods for measuring the ION cross-sectional area suffer from motion related problems associated with long acquisition times but also from operator dependent errors arising at the time of image analysis. This study has used a multi-dynamic acquisition scheme followed by image registration of the individual volumes into a single, more conspicuous image that was used for measuring the mean-cross sectional area of the entire ION. In addition, this study has shown that the use of a well established image segmentation method, currently used for spinal cord cross-sectional area measurements (16), could also be applied when assessing the optic nerves.

The MR image acquisition protocol implemented in this study took into account a number of technical considerations. The choice of a coronal-oblique prescription of the imaging volume was important to ensure orthogonal sections through the ION and a reduction of through plane partial volume effects. The use of a multi-dynamic acquisition scheme was important to ensure that motion related problems, usually associated with longer acquisition times, would be improved considerably. A key characteristic of the acquisition scheme is related to the option of adding further dynamics to the protocol, either in situations when motion is identified on some of the dynamic acquisitions (i.e. in real time) or to reach significant signal-to-noise which is hardware dependent (e.g. due to main magnetic field strength constraints or head coil options available). In any case, the

acquisition scheme presented in this study required no additional software or hardware pertaining to the MR system and as such this could be easily translated into the clinical setting. However, the method requires to a great extend the co-operation of the volunteer and this may be a limiting factor in certain applications.

To our knowledge, the use of ASM for segmenting the entire ION has not been reported previously; this study has shown that this segmentation method can have important applications in optic nerve imaging. The method is fast, easy to use and it reduces considerably the manual editing required during the analysis. Importantly, it facilitates measurements of the mean cross-sectional area of the optic nerves, as opposed to the mean diameter, which is believed to be a more representative measure of atrophy, as has been previously described (16). The mean intra-observer COV value of 2% (i.e. average of the left and right ION measurements) identified from the reproducibility study is considerably lower than previously reported values of 2.1% - 4.8% for a portion of the ION only (5, 12); our result is encouraging and supportive of future applications. However, the intra-observer COV value identified in this study is considerably higher than that reported in a study measuring the healthy spinal cord cross-sectional area using the same analysis method (i.e. 0.59%) (16). This, however, is likely to be due to the small size of the optic nerve, the greater potential for motion artefacts and the difference in signal-to-noise ratio. Future work on a larger sample population will confirm the performance of the segmentation method presented here for measuring the cross-sectional area of the entire ION; further improvements are likely to depend primarily on the signal-to-noise ratio and the resolution of the acquisition.

Normative mean cross-sectional area measurements of the ION obtained with the proposed acquisition and analysis protocol are in agreement with other studies, with the ION naturally reducing in diameter as it extends from the globe towards the orbital apex (9-14). However, a direct comparison of the cross-sectional area measurement values obtained in this study with the ones obtained from other MR investigations is not straightforward. Studies have shown that there is a variation in the amount of extrafascicular matrix between subjects, especially the amount of collagen nearest to the globe (9). On the other hand, methodological factors such as the type of image contrast (e.g. T1-weighted or T2-weighted), the segment of the optic nerve studied, the image resolution and the type of mage analysis can all hinder the interpretation of normative data across different studies.

There is little doubt that for any given acquisition and analysis protocol to have successful clinical utility, certain important conditions must be met. For example, the acquisition and analysis protocol ought to be faster that existing protocols, must be easily implemented without additional software or hardware requirements, but most importantly must offer reproducible results from repeated measurements. In this study, the mean scan-rescan COV value was calculated as 4.4%, which is lower than previously reported values of 4.9% - 6.5% using multi-slice acquisitions (5, 6, 12). While the COV values identified in this study are lower than previous reports, there is scope for improving this result. Signal-to-noise ratio is currently the main limiting factor, hence future work will be directed at improving this, possibly by evaluating different coil designs as well as further refining the acquisition scheme.

The ability to detect small changes in cross-sectional area of the ION may have important implications for monitoring disease changes. However, cross-sectional area measurements in disease state may prove less straightforward than the study of healthy subjects. For example in MS, following an episode of optic neuritis, the lesion is likely to be different in appearance and diameter when assessed using T2- and T1-weighted acquisitions; reports have shown that swelling may occur following an episode of unilateral optic neuritis which is likely to progress into atrophy at a later stage (5, 6). It is therefore suggested that studies are conducted specifically to assess the potential value of the method presented here for measuring atrophy in longitudinal studies of optic neuritis and compared with more traditional measurement methods (5-8). The most important quality of the present acquisition and analysis protocol, besides the improved reproducibility, is the fact that the entire ION can be assessed in a single imaging session, unlike existing imaging protocols that do not routinely offer this option.

In summary, this study defines a protocol from image acquisition to data analysis for reproducible measurements of the mean cross-sectional area of the ION in healthy volunteers that can be used in the clinical setting to study pathological conditions that affect the ION.

REFERENCES

1. Lagrèze WA, Gaggl M, Weigel M, et al. Retrobulbar optic nerve diameter measured by high-speed magnetic resonance imaging as a biomarker for axonal loss in glaucomatous optic atrophy. Invest Ophthalmol Vis Sci. 2009;50(9):4223-4228.
2. Beatty S, Good PA, McLaughlin J, O'Neill EC. Echographic measurements of the retrobulbar optic nerve in normal and glaucomatous eyes. Br J Ophthalmol. 1998;82(1):43-47.
3. Stroman GA, Stewart WC, Golnik KC, Curé JK, Olinger RE. Magnetic resonance imaging in patients with low-tension glaucoma. Arch Ophthalmol. 1995;113(2):168-172.
4. Kashiwagi K, Okubo T, Tsukahara S. Association of magnetic resonance imaging of anterior optic pathway with glaucomatous visual field damage and optic disc cupping. J Glaucoma. 2004;13(3):189-195.
5. Hickman SJ, Brex PA, Brierley CMH, et al. Detection of optic nerve atrophy following a single episode of unilateral optic neuritis by MRI using a fat-saturated short-echo fast FLAIR sequence. Neuroradiology. 2001;43(2):123-128.
6. Hickman SJ, Toosy AT, Jones SJ, et al. A serial MRI study following optic nerve mean area in acute optic neuritis. Brain. 2004;127(Pt 11):2498-2505.
7. Hickman SJ. Optic nerve imaging in multiple sclerosis. J Neuroimaging. 2007;17 Suppl.1: 42S-45S.
8. Hickman SJ, Miszkiel KA, Plant GT, Miller DH. The optic nerve sheath on MRI in acute optic neuritis. Neuroradiology. 2005;47(1):51-55.

9. Karim S, Clark RA, Poukens V, Demer JL. Demonstration of systematic variation in human intraorbital optic nerve size by quantitative magnetic resonance imaging and histology. Invest Ophthalmol Vis Sci. 2004;45(4):1047-1051.
10. Weigel M, Lagrèze WA, Lazzaro A, Hennig J, Bley TA. Fast and quantitative high-resolution magnetic resonance imaging of the optic nerve at 3.0 tesla. Invest Radiol. 2006;41(2):83-86.
11. Lagrèze WA, Lazzaro A, Weigel M, Hansen HC, Hennig J, Bley TA. Morphometry of the retrobulbar human optic nerve: comparison between conventional sonography and ultrafast magnetic resonance sequences. Invest Ophthalmol Vis Sci. 2007;48(5):1913-1917.
12. Yiannakas MC, Wheeler-Kingshott CA, Berry AM, et al. A method for measuring the cross sectional area of the anterior portion of the optic nerve in vivo using a fast 3D MRI sequence. J Magn Reson Imaging. 2010;31(6):1486-1491.
13. Ozgen A, Aydingöz U. Normative measurements of orbital structures using MRI, J Comput Assist Tomogr. 2000;24(3):493-496.
14. Bert RJ, Patz S, Ossiani M, et al. High-resolution imaging of the human eye 2005. Acad Radiol. 2006;13(3):368-378.
15. Walsh FB. The visual sensory system. In Walsh FB, Hoyt WF (eds). Clinical neuro-ophthalmolohy, 3rd edition. Baltimore: Williams and Wilkin; 1969: p. 1-129.
16. Horsfield MA, Sala S, Neema M, et al. Rapid semi-automatic segmentation of the spinal cord from magnetic resonance images: application in multiple sclerosis. Neuroimage. 2010;50(2):446-455.

17. Otsu, N. A Threshold Selection Method from Gray-Level Histograms. IEEE Transactions on Systems, Man, and Cybernetics, 1979;9(1):62-66.

Figure 1. Coronal-oblique orthogonal sections through the intraorbital optic nerve (ION) facilitated by high-resolution reference images acquired in a) the sagittal plane and b) the axial plane; imaging of the right ION is shown in this example.

Figure 2. a) Coronal-oblique T2-weighted image of the left intraorbital nerve (ION) acquired with a single dynamic scan in 32 seconds highlighting the region that was cropped from each slice prior to the image registration step and b) the final cropped image.

Figure 3. a) Example of a single slice taken from repeatedly acquired volumes (i.e. each volume acquired in 32 seconds) in the anterior portion of the intraorbital optic nerve (i.e. proximal 3 mm to the globe) and added following interpolation and binarization; note the degree of misalignment between slices in this example, despite the co-operation of the participant by focusing their vision on a colored marker in straight gaze b) the final image following 2D image registration and addition of the slices.

Figure 4. Example of the active surface model (ASM) segmetation method; a) single seed points were initially positioned within the intraorbital optic nerve in consecutive slices b) the boundary of the optic nerve was then identified by the algorithm; no manual intervention was required in this example following boundary identification; c) example of the final image shown in b), which is shown following interpolated to higher resolution in order to improve the display.

Table 1. Mean cross-sectional area measurements and scan –rescan reproducibility results for the left and right intraorbital optic nerves (ION) in 5 healthy volunteers*.

Left ION				Right ION			
Slice No.; distance from the globe (mm)	Number of subjects	Mean (SD) cross-sectional area (mm^2)	Scan-rescan COV (%)	Slice No.; distance from the globe (mm)	Number of subjects	Mean (SD) cross-sectional area (mm^2)	Scan-rescan COV (%)
Slice 1; 0-3	5/5	7.8 (1.6)	3.3	Slice 1; 0-3	5/5	8 (1.5)	3.3
Slice 2; 3-6	5/5	6.2 (1.3)	9.4	Slice 2; 3-6	5/5	6.7 (0.9)	7.1
Slice 3; 6-9	5/5	5.2 (1)	8.4	Slice 3; 6-9	5/5	5.8 (0.9)	5.4
Slice 4; 9-12	5/5	4.7 (0.7)	6.2	Slice 4; 9-12	5/5	5.2 (0.9)	7
Slice 5; 12-15	5/5	4.4 (0.6)	9	Slice 5; 12-15	5/5	4.9 (0.8)	9.1
Slice 6; 15-18	5/5	4.2 (0.6)	10.6	Slice 6; 15-18	5/5	4.6 (0.6)	9.4
Slice 7; 18-21	5/5	4.1 (0.9)	8.6	Slice 7; 18-21	5/5	4.4 (0.6)	8.7
Slice 8; 21-24	5/5	3.8 (1)	4.4	Slice 8; 21-24	5/5	4.2 (0.9)	8.1
Slice 9; 24-27 (Apex level for 3/5 subjects)	3/5	4.2 (1.6)	8.3	Slice 9; 24-27 (Apex level for 3/5 subjects)	3/5	4.5 (1.2)	13.2

* Results shown are for each section of the ION (i.e. slice by slice) starting from immediately behind the globe to the apex; reproducibility results shown are from the scan-rescan assessment.

Figure 1.

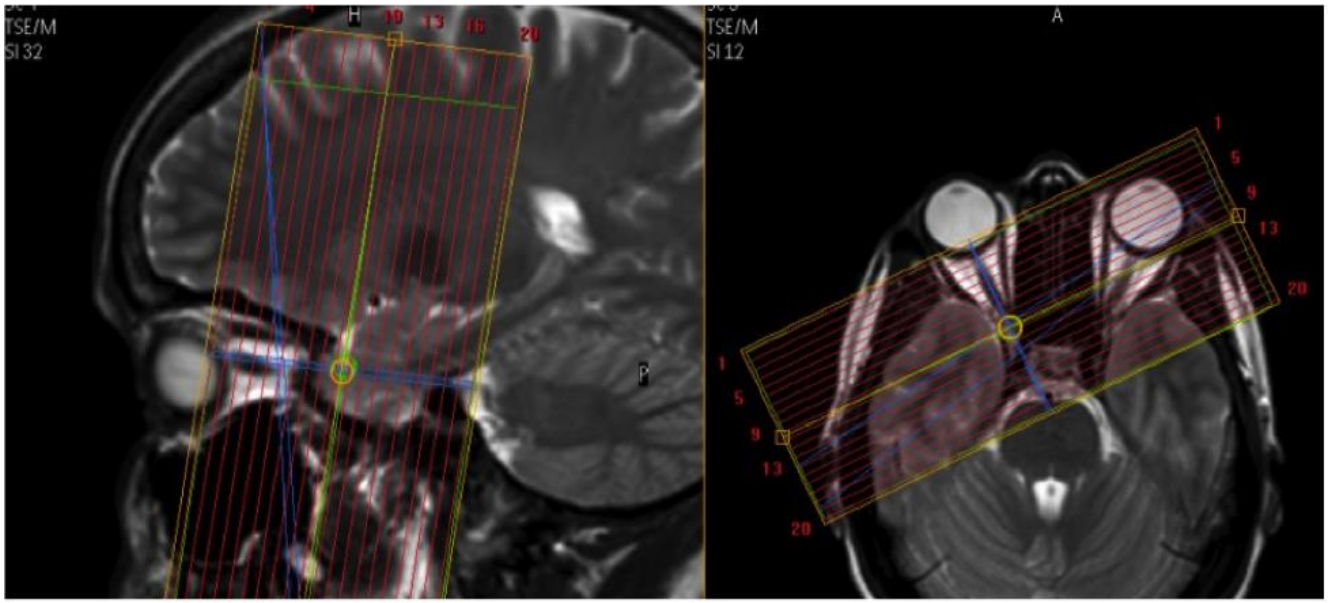

a) b)

Figure 2.

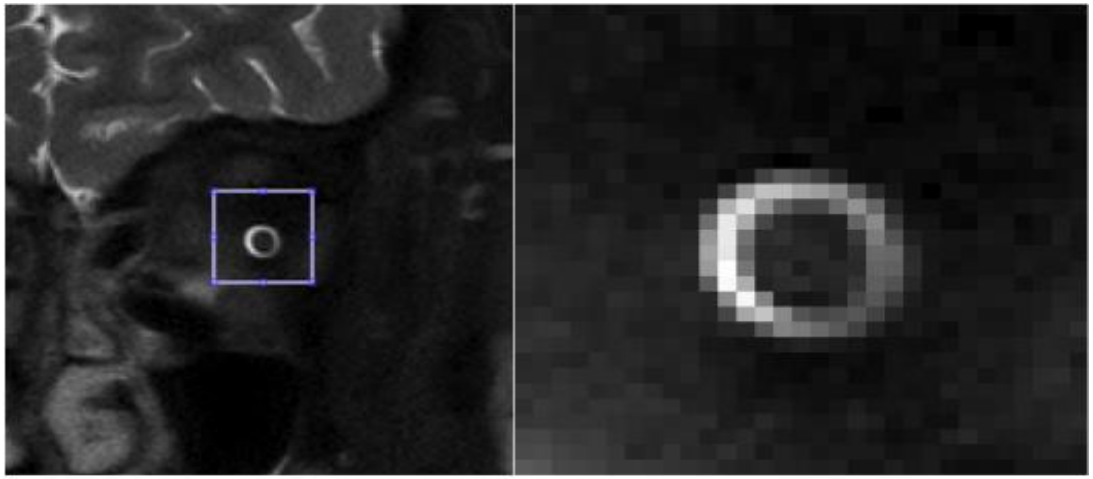

a) b)

Figure 3.

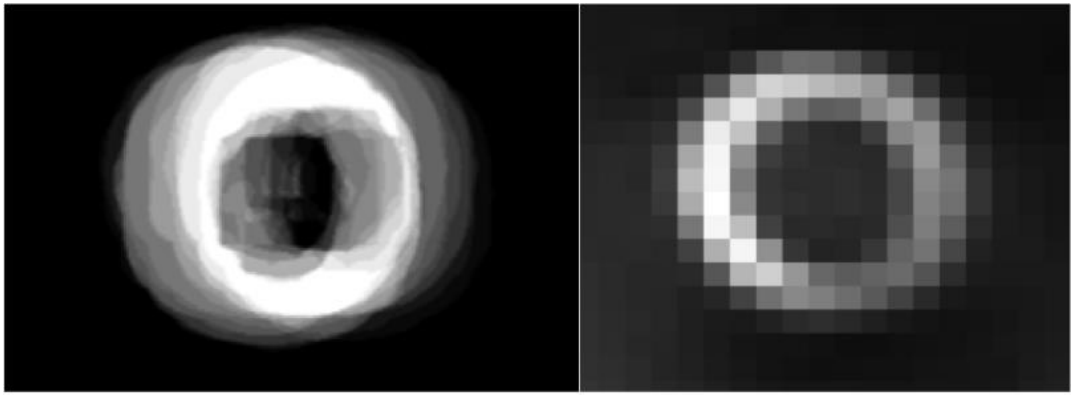

a) b)

Figure 4.

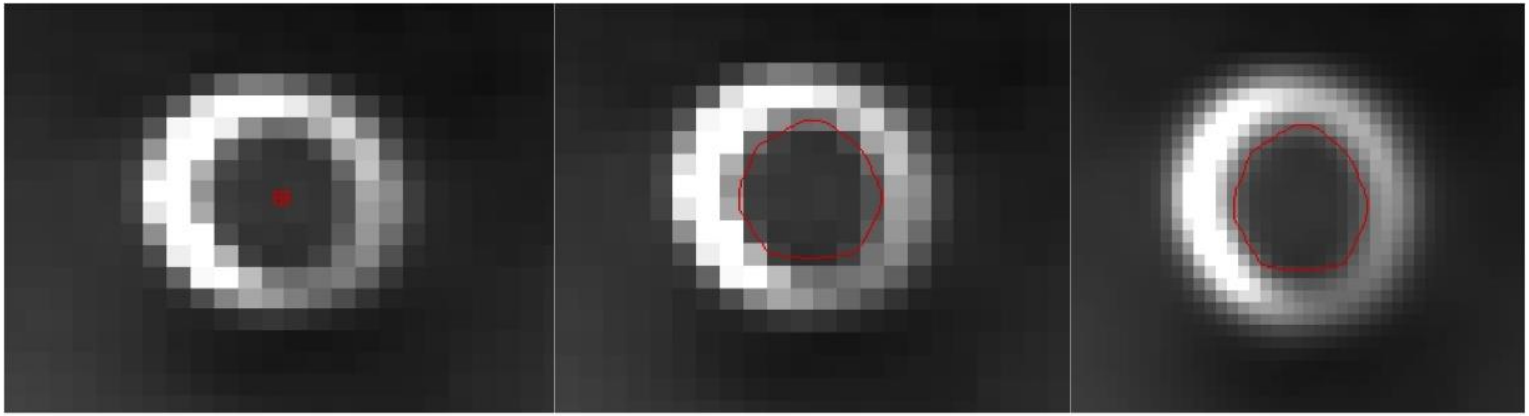

a) b) c)